

Theoretical analysis of ultra-lean premixed flames in porous inert media

F. M. PEREIRA¹†, A. A. M. OLIVEIRA¹ AND F. F. FACHINI²

¹Departamento de Engenharia Mecânica, Universidade Federal de Santa Catarina, 88040-900 Florianópolis, SC, Brazil

²Laboratório de Combustão e Propulsão, Instituto Nacional de Pesquisas Espaciais, 12630-000 Cachoeira Paulista, SP, Brazil

(Received 30 September 2009; revised 10 March 2010; accepted 16 March 2010;
first published online 10 June 2010)

The structure of stationary adiabatic premixed flames within porous inert media under intense interphase heat transfer is investigated using the asymptotic expansion method. For the pore sizes of interest for combustion in porous inert media, this condition is reached for extremely lean mixtures where lower flame velocities are found. The flame structure is analysed in three distinct regions. In the outer region (the solid-phase diffusion length scale), both phases are in local thermal equilibrium and the problem formulation is reduced to the one-equation model for the energy conservation. In the first inner region (the gas-phase diffusion length scale), there is local thermal non-equilibrium and two equations for the energy conservation are required. In this region, the gas-phase temperature at the flame is limited by the interphase heat transfer. In the second inner region (the reaction length scale), the chemical reaction occurs in a very thin zone where the highest gas-phase temperature is found. The results showed that superadiabatic effects are reduced for leaner mixtures, smaller pore sizes and smaller fuel Lewis numbers. The results also show that there is a minimum superadiabatic temperature for the flame propagation to be possible, which corresponds to the lean flammability limit for the premixed combustion in porous inert media. A parameter that universalizes the leading-order flame properties is identified and discussed.

Key words: flames, laminar reacting flows, porous media

1. Introduction

Lean premixed combustion in porous inert media has received much attention in the last few decades as a way of extending flame stability, burning low-heat-content fuels and providing radiant heating (Howell, Hall & Ellzey 1996; Oliveira & Kaviany 2001). The heat recirculation induced by the porous media adds to the energy released by combustion resulting in local temperatures in excess of the adiabatic flame temperature for the gas phase, a phenomenon that has been called superadiabatic combustion (Echigo 1991). This high temperature in the reaction region increases the reaction rate and allows for combustion of low-heat-content gas mixtures whose stoichiometric ratio lies outside the flammability limits for unstretched laminar free flames.

† Email address for correspondence: fernando@labcet.ufsc.br

In this work, ultra-lean premixed flames within infinite adiabatic porous inert media are studied analytically. This condition is characterized by low flame velocities that result in intense interphase heat transfer, which in turn leads to thermal equilibrium between the gas and solid phases in a wide region around the flame. The analysis shows that this intense interphase heat transfer limits the superadiabatic effect and reveals thermal aspects of the lean flammability limit for the flame propagation in porous inert media.

There is a lack of studies concerning the steady-state ultra-lean operation of porous burners (Wood & Harris 2008). In an experimental and numerical study of radiant porous burners performance, Hsu, Evans & Howell (1993) obtained stable methane–air flames at equivalence ratios as low as 0.41, which is smaller than the lean flammability limit for free flames, $\phi = 0.5$ (Law 2006). The results showed that there was a decreasing flow rate range where stable flames could be sustained as the mixture was made leaner. Below a certain value of the equivalence ratio ($\phi \leq 0.55$) the burner heat loss was the dominating factor in determining the minimum flow rate for stable flames. In these cases, the flame did not present flashback: instead, it just extinguished when the flow rate was decreased. Although the experiments could not reach the flammability limit, the authors hypothesized that, at this limit, there is only one flow rate that leads to a stable flame. For this flow rate, the energy released by the combustion process is just large enough to yield the temperature required to maintain the chemical reaction. This means that, for the ultra-lean operation of radiant burners, the lean flammability limit is determined by a balance between heat losses and heat recirculation. Experimental and numerical studies have reported stable flames below the unstretched laminar free-flame lean flammability limit (Min & Shin 1991; Hackert, Ellzey & Ezekoye 1999; Liu & Hsieh 2004). It is expected that, for perfectly adiabatic burners, the lean limit for the flame propagation will be found for much lower equivalence ratios than in radiant burners. Other experimental works report stable ultra-lean combustion in porous inert media (Hardesty & Weinberg 1974; Kotani & Takeno 1982; Kotani, Behbahani & Takeno 1984), but some kind of external heat recirculation is used.

Ultra-lean combustion is also achieved in low-velocity forward filtration combustion in porous inert media (Zhdanok, Kennedy & Koester 1995; Henneke & Ellzey 1999; Shi *et al.* 2008). In this case, the reaction front propagates at low velocities (less than 1 mm s^{-1}) and the flame can be sustained for equivalence ratios as low as 0.15. The interaction of the combustion wave with the thermal wave can lead the flame to reach temperatures as high as 2.8 times the corresponding adiabatic flame limit (Zhdanok *et al.* 1995). For the case of reciprocal flow filtration combustion reactors, lean flammability limits are found for equivalence ratios as low as 0.026 (Hoffmann *et al.* 1997) due to the intense heat recuperation induced by this system. Dobrego *et al.* (2008) present a numerical study of the influence of several parameters on the lean flammability limit for methane–air mixtures in reciprocating combustion. This is not the case for stationary flames. As it will be shown below, the non-dimensional flame temperature based on the adiabatic flame temperature decreases as the flammability limit is approached.

Asymptotic analyses have been proposed for the solution of the stationary premixed gas flames within porous inert media for semi-infinite and finite length burners (Deshaies & Joulin 1980; Buckmaster & Takeno 1981; McIntosh 1988; Golombok *et al.* 1991; McIntosh & Prothero 1991; Boshoff-Mostert & Viljoen 1996; Schoegl & Ellzey 2007). All these models divide the flame in a preheating region, a thin combustion region and a post-combustion region. Expressions for the gas- and solid-phase temperatures and flame position are obtained as a function of an imposed

flame velocity. Analytical solutions for the problem of filtration combustion in porous inert media (Zhdanok *et al.* 1995; Bubnovich, Zhdanok & Dobrego 2006) and in porous reactive media (Schultz *et al.* 1996; Wahle & Matkowsky 2001) are also proposed in the literature.

In a previous work (Pereira, Oliveira & Fachini 2009), an asymptotic solution was proposed for stationary adiabatic premixed flames in porous inert media taking advantage of the large difference between the thermal conductivity of the solid and gas phases. In that analysis, a two-equation model for the energy conservation is used with effective properties and a diffusion approximation for the intramedium radiation. The flame structure is characterized by three characteristic length scales. The two innermost length scales are the same scales defined in the classical premixed flame structure analysis. The outermost length scale is related to the heat conduction in the porous matrix. The results of the model show that the influence of the porous medium on the flame is to increase its temperature and velocity and that this influence is more pronounced for leaner mixtures, higher solid-phase thermal conductivities, lower porosities and lower fuel Lewis numbers. It is also shown that the reaction region is shorter in flames within porous media since higher flame temperatures are found.

The previous work is valid for equivalence ratios ranging approximately from 0.60 to 0.80. The upper bound is the result of the simplifications involved in the one-step kinetic mechanism used. The lower bound is related to an interphase heat transfer parameter defined as $N \equiv \lambda_s h_v / (\rho_n s_F c_p)^2$, where λ_s is the solid-phase effective thermal conductivity, h_v is the volumetric surface convection coefficient, ρ_n is the unburnt gas-phase density, s_F is the flame velocity measured in the unburned stream and c_p is the gas-phase heat capacity at constant pressure. In that analysis the condition $N \ll \Gamma$ is satisfied, where Γ is the thermal conductivities ratio ($\Gamma = \lambda_s / \lambda_g$, where λ_g is the gas-phase effective thermal conductivity). Typical values of Γ range from 10 to 300 depending on the matrix conductivity and structure. Then, with $N \sim O(1)$, the specific condition analysed in the previous work, the interphase heat transfer at the gas phase and at the reaction length scales is negligible. Then, the flame structure at the inner scales is similar to that of a free flame. This will not hold for extremely lean mixtures where lower flame velocities are found.

The present study aims to extend the previous work to lower equivalence ratios where the condition $N \sim O(\Gamma)$ prevails. Higher values of N result in local thermal equilibrium between the phases in a wide region around the flame. This intense interphase heat transfer limits the superadiabatic effect, showing that the superadiabatic flame temperature should have a maximum at the lean side of the equivalence ratio range. The model also provides a first approximation for the lean flammability limit for the flame propagation in adiabatic porous inert media based on thermal considerations. In this case, since there is no influence of heat losses, the lean flammability limit is determined only by the heat recirculation that is a function of the solid- and gas-phase properties. To the authors' knowledge, an analysis of these limits has not been reported before.

2. Length scales and thermal non-equilibrium

Figure 1 shows a schematic representation of the problem under consideration. Since we are dealing with extremely lean mixtures with very low flame velocities, the gas and solid phases have enough contact time to reach thermal equilibrium in a wide region around the flame. This region corresponds to a characteristic solid-phase diffusion length scale defined as $l_s \equiv (1 - \varepsilon)\lambda_s / (\varepsilon\rho_n s_F c_p)$, where ε is the volumetric

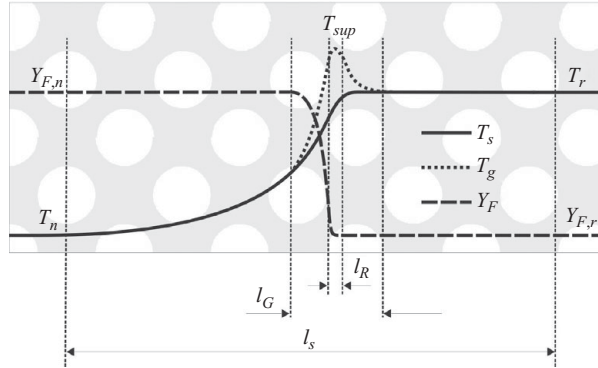


FIGURE 1. Schematic representation of the temperatures and fuel mass fraction distributions and the different characteristic length scales of the problem.

porosity. In a thin region around the flame there is still considerable thermal non-equilibrium between the phases. This region corresponds to a characteristic gas-phase diffusion length scale defined as $l_G \equiv \varepsilon \lambda_g / (\varepsilon \rho_n s_F c_p)$. The ratio between these two scales is $l_G/l_S \sim \varepsilon/\Gamma(1-\varepsilon)$. As in the previous work, the present model is restricted to $\varepsilon/(1-\varepsilon) \sim O(1)$, ensuring the scales separation ($l_G/l_S \sim 1/\Gamma$).

As the equivalence ratio decreases, the larger contact time between the phases causes an intense heat transfer from the gas phase to the solid phase at the length scale l_G . Then, contrary to the previous model, the non-dimensional flame temperature decreases as the mixture is made leaner. Since the flame velocity is proportional to the Lewis number, the same results are found when the Lewis number is decreased. These behaviours are particular to ultra-lean premixed combustion in porous inert media and are due to a change in the direction of the interphase heat transfer. For higher flame velocities, the interphase heat transfer is important only at the solid-phase diffusion length scale l_S where, upstream from the flame, the solid phase loses heat to the gas phase. For lower flame velocities, both phases are in local thermal equilibrium at the length scale l_S and the interphase heat transfer is intense at the gas-phase diffusion length scale l_G . Now, upstream from the flame, it is the gas phase that loses heat to the solid phase.

The description of the reaction region is identical to the previous work since the interphase heat transfer in this region is still negligible. Here a characteristic reaction length scale is defined as $l_R/l_G \equiv \delta$. The parameter δ is the inverse of a modified Zel'dovich number defined as $1/\delta = (E_a(T_r - T_n))/(R_u T_{sup}^2)$, where R_u is the universal gas constant, E_a is the activation energy, according to the Arrhenius reaction rate model, T_{sup} is the superadiabatic flame temperature (maximum temperature at the reaction region) and T_n is the initial temperature.

The heat transfer parameter $N \equiv \lambda_s h_v / (\rho_n s_F c_p)^2$ controls the degree of non-equilibrium between the phases in each one of the characteristic length scales defined above. As $N \rightarrow \infty$, the solid and gas phases tend to thermal equilibrium in all length scales and a single temperature could be used to model the problem. As $N \rightarrow 0$, the interphase heat transfer becomes negligible everywhere and the problem reduces to a free-flame structure for the gas phase that is totally decoupled from the solid-phase temperature.

The order of magnitude of the parameter N is determined by $N \sim \tau_S/\tau_h$, where $\tau_S = l_S/s_F$ is the characteristic residence time at the solid-phase diffusion length scale

and $\tau_h = \rho_n c_p / h_v$ is the characteristic time for heat transfer. Characteristic time scales can be similarly defined for the inner scales as $\tau_G = l_G / s_F$ and $\tau_R = l_R / s_F$. Then, for $N \sim O(1)$, the case analysed in the previous work, we have $\tau_S \sim \tau_h$, $\tau_G \sim \tau_h / \Gamma$ and $\tau_R \sim \tau_h \delta / \Gamma$, which means that the residence times at the inner scales are very small compared to the heat transfer time. As a result, the interphase heat transfer is important at the outermost length scale l_S only. In the present work, since $N \sim O(\Gamma)$, we now have $\tau_S \sim \tau_h \Gamma$, $\tau_G \sim \tau_h$ and $\tau_R \sim \tau_h \delta$. Then, the interphase heat transfer is still negligible at the innermost length scale l_R , whereas it is important at the intermediate length scale l_G . At the outermost length scale l_S , however, the residence time is much larger than the time for heat transfer, so thermal equilibrium between the phases is reached. For the case $N \sim O(\Gamma / \delta)$, to be discussed in a future work, the interphase heat transfer is important at l_R only, and thermal equilibrium is reached at the outer scales.

For a given value of Γ and fluid properties, the characteristic residence time is basically determined by the flame velocity s_F , whereas the time for heat transfer is basically determined by the volumetric heat transfer coefficient h_v . Then, higher values of N may be reached by decreasing the equivalence ratio, resulting in lower flame velocities, or, for a fixed porosity, decreasing the pore size of the solid matrix, resulting in higher values of h_v . Note, however, that s_F and h_v are not independent parameters and N is subjected to many cross-influences. In the present model, we choose to work with pore sizes of the order of 1 mm, which are typical of porous burners with submerged flames, so the condition $N \sim O(\Gamma)$ may be reached by decreasing the equivalence ratio. Discussions about the conditions that lead to thermal non-equilibrium in combustion of porous reactive media and of porous solid propellants are found in Wahle, Matkowsky & Aldushin (2003) and Telengator, Williams & Margolis (2006), respectively.

From the asymptotic point of view, the flame structure analysis follows the hypothesis that $l_S \gg l_G \gg l_R$. Moreover, from the point of view of the use of a continuous treatment for the porous medium (Kaviany 1995), it is assumed that $l_S \gg l_{rev} \gg l_d$, where l_{rev} is the characteristic length of the representative elementary volume over which the volume-averaging is done and l_d is the characteristic length of the pores. Contrary to the previous model, in the present analysis the gas-phase diffusion length scale is larger than the pore size while the reaction length scale is still confined to a single pore, $l_G > l_d > l_R$. Then, the innermost length scale l_R behaves as a subgrid model with negligible interphase heat transfer.

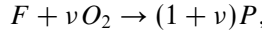
In the following, the equations for the model are written and solved using the asymptotic expansion method. The solution for the innermost scale follows the large activation energy asymptotic method (Liñán 1974; Fachini 1996; Fachini, Liñán & Williams 1999; Fachini 2005). Finally, typical results are presented and discussed in view of the model.

3. Mathematical formulation

A one-dimensional two-medium model for the conservation of mass, mass of chemical species, gas-phase energy and solid-phase energy is constructed, following Pereira *et al.* (2009). The mass conservation implies that $\rho_n u_n$ is constant for the one-dimensional flow with u_n being the gas velocity far upstream from the flame. For stationary flames, the laminar flame speed s_F is equal to u_n . The gas-phase specific heat capacity c_p , the effective thermal conductivities ($\varepsilon \lambda_g$ for the gas and $(1 - \varepsilon) \lambda_s$ for the solid) and the product $\rho \varepsilon D_i$ (gas-phase density times effective mass diffusivity

of species i) are assumed uniform along the flame. The effective thermal conductivity of the solid phase includes the pore tortuosity and the intraphase radiation through a radiant conductivity (Rosseland approximation). The effective thermal conductivity and mass diffusivity of the gas phase include the pore tortuosity and the hydrodynamic dispersion effects. The gas-phase radiation and flame stretch effects are neglected. The pressure drop across the porous medium is assumed negligible when compared to the total pressure and the momentum equation becomes trivial.

The fuel combustion is assumed to occur following a global one-step mechanism, represented in mass variables as



where ν is the mass of oxygen per mass of fuel ratio (stoichiometric).

The steady-state volume-averaged mass, energy and species conservation equations (omitting for simplicity the volume-averaging notation) then become

$$\varepsilon \rho u = \varepsilon \rho_n s_F, \quad (3.1)$$

$$\varepsilon \rho_n s_F \frac{dY_F}{dx} = \varepsilon \rho D_F \frac{d^2 Y_F}{dx^2} - \varepsilon A \rho^2 Y_O Y_F T_g^a e^{-E_a/R_u T_g}, \quad (3.2)$$

$$\varepsilon \rho_n s_F \frac{dY_O}{dx} = \varepsilon \rho D_O \frac{d^2 Y_O}{dx^2} - \varepsilon \nu A \rho^2 Y_O Y_F T_g^a e^{-E_a/R_u T_g}, \quad (3.3)$$

$$\varepsilon \rho_n s_F c_p \frac{dT_g}{dx} = \varepsilon \lambda_g \frac{d^2 T_g}{dx^2} + \varepsilon Q A \rho^2 Y_O Y_F T_g^a e^{-E_a/R_u T_g} + h_v(T_s - T_g), \quad (3.4)$$

$$0 = (1 - \varepsilon) \lambda_s \frac{d^2 T_s}{dx^2} - h_v(T_s - T_g), \quad (3.5)$$

where Y_F and Y_O are the gas-phase volume-averaged fuel and oxidant mass fractions, εD_F and εD_O are the fuel and oxidant total effective mass diffusivities, T_g and T_s are the gas-phase and solid-phase phasic volume-averaged temperatures, Q is the fuel, mass, based heat of reaction, A is the pre-exponential factor of the Arrhenius reaction rate and a is the temperature exponent of the reaction rate expression.

3.1. Non-dimensionalization

Defining the non-dimensional variables (Williams 1985)

$$y_F \equiv \frac{Y_F}{Y_{Fn}}, \quad y_O \equiv \frac{Y_O}{Y_{On}}, \quad \theta \equiv \frac{c_p(T - T_n)}{Y_{Fn} Q} = \frac{T - T_n}{T_r - T_n} \quad \text{and} \quad \zeta \equiv \int_0^x \frac{\rho_n s_F}{\lambda_s/c_p} dx,$$

equations (3.2)–(3.5) become

$$\varepsilon \frac{dy_F}{d\zeta} = \frac{\varepsilon}{Le_F \Gamma} \frac{d^2 y_F}{d\zeta^2} - \varepsilon \Gamma Da y_O y_F \exp \left[-\frac{\beta(1 - \theta_g)}{1 - \alpha(1 - \theta_g)} \right], \quad (3.6)$$

$$\varepsilon \frac{dy_O}{d\zeta} = \frac{\varepsilon}{Le_O \Gamma} \frac{d^2 y_O}{d\zeta^2} - \varepsilon \phi \Gamma Da y_O y_F \exp \left[-\frac{\beta(1 - \theta_g)}{1 - \alpha(1 - \theta_g)} \right], \quad (3.7)$$

$$\varepsilon \frac{d\theta_g}{d\zeta} = \frac{\varepsilon}{\Gamma} \frac{d^2 \theta_g}{d\zeta^2} + \varepsilon \Gamma Da y_O y_F \exp \left[-\frac{\beta(1 - \theta_g)}{1 - \alpha(1 - \theta_g)} \right] + N(\theta_s - \theta_g), \quad (3.8)$$

$$0 = (1 - \varepsilon) \frac{d^2 \theta_s}{d\zeta^2} - N(\theta_s - \theta_g), \quad (3.9)$$

where

$$\Gamma \equiv \frac{\lambda_s}{\lambda_g}, \quad \phi \equiv \frac{Y_{Fn} v}{Y_{On}}, \quad \alpha \equiv \frac{(T_r - T_n)}{T_r}, \quad \beta \equiv \frac{E_a(T_r - T_n)}{R_u T_r^2},$$

$$Le_i \equiv \frac{\lambda_g}{\rho_n c_p D_i}, \quad Da \equiv \frac{A \rho^2 \lambda_g Y_{On} T_g^a \exp(-\beta/\alpha)}{(\rho_n^2 s_F^2 c_p)},$$

and $N \equiv \frac{\lambda_s h_v}{(\rho_n s_F c_p)^2}.$

The parameter ϕ is the equivalence ratio, α is the dimensionless heat release, β is the Zel'dovich number, Le_i is the species i effective Lewis number that accounts for the thermal and species hydrodynamic dispersions (i stands for fuel F and oxidant O), Da is the Damköhler number and N is the interphase heat transfer parameter.

To achieve ultra-lean premixed flames, the burning conditions are such that the value of the interphase heat transfer parameter N becomes very large, $N \gg 1$. In the present work, the condition $N \sim O(\Gamma)$ is chosen in order to observe the response of the flame properties to the thermal non-equilibrium between the phases in the gas-phase diffusion length scale l_G .

In the following, the problem of the order of unity, corresponding to the solid-phase diffusion length scale l_s , is solved. Then, the problem of the order of Γ^{-1} , corresponding to the gas-phase diffusion length scale l_G , is solved. Finally, the problem of the order of $\delta\Gamma^{-1}$, corresponding to the reaction length scale l_R , is solved.

3.2. Outer zone: problem of the order of unity

In the characteristic length scale $\zeta - \zeta_f \sim O(1)$, the diffusive terms in the gas phase are of the order of Γ^{-1} and the reaction is exponentially small. Thus, equations (3.6)–(3.9) take the form

$$\varepsilon \frac{dy_F}{d\zeta} = \frac{\varepsilon}{Le_F \Gamma} \frac{d^2 y_F}{d\zeta^2}, \tag{3.10}$$

$$\varepsilon \frac{dy_O}{d\zeta} = \frac{\varepsilon}{Le_O \Gamma} \frac{d^2 y_O}{d\zeta^2}, \tag{3.11}$$

$$\varepsilon \frac{d\theta_g}{d\zeta} = \frac{\varepsilon}{\Gamma} \frac{d^2 \theta_g}{d\zeta^2} + N(\theta_s - \theta_g), \tag{3.12}$$

$$0 = (1 - \varepsilon) \frac{d^2 \theta_s}{d\zeta^2} - N(\theta_s - \theta_g). \tag{3.13}$$

The solution of (3.10)–(3.13) can be written as

$$\left. \begin{aligned} y_F &= y_F^{(0)} + \Gamma^{-1} y_F^{(1)} + o(\Gamma^{-1}), \\ y_O &= y_O^{(0)} + \Gamma^{-1} y_O^{(1)} + o(\Gamma^{-1}), \\ \theta_s &= \theta_s^{(0)} + \Gamma^{-1} \theta_s^{(1)} + o(\Gamma^{-1}), \\ \theta_g &= \theta_g^{(0)} + \Gamma^{-1} \theta_g^{(1)} + o(\Gamma^{-1}). \end{aligned} \right\} \tag{3.14}$$

Substituting (3.14) into (3.10)–(3.13) and applying the limit $\Gamma \rightarrow \infty$ ($N \rightarrow \infty$), the first approximation for the set of equations of the order of unity is

$$\frac{dy_F^{(0)}}{d\zeta} = 0, \tag{3.15}$$

$$\frac{dy_O^{(0)}}{d\zeta} = 0, \quad (3.16)$$

$$\theta_s^{(0)} = \theta_g^{(0)} = \theta^{(0)}. \quad (3.17)$$

The boundary conditions for $\zeta \rightarrow -\infty$ are $\theta^{(0)} = 0$ and $y_F^{(0)} = y_O^{(0)} = 1$ and for $\zeta \rightarrow +\infty$ are $\theta^{(0)} = 1$ and $y_F^{(0)} = y_O^{(0)} - (1 - \phi) = 0$. The solutions for (3.15) and (3.16) are $y_F^{(0)} = y_O^{(0)} = 1$ for $\zeta < \zeta_f$ and $y_F^{(0)} = 0$ and $y_O^{(0)} = 1 - \phi$ for $\zeta > \zeta_f$.

Summing up (3.12) and (3.13), imposing the thermal equilibrium condition (3.17) and neglecting the term of the order of $1/\Gamma$, one finds

$$\frac{d\theta^{(0)}}{d\zeta} = \left(\frac{1 - \varepsilon}{\varepsilon} \right) \frac{d^2\theta^{(0)}}{d\zeta^2}. \quad (3.18)$$

Equation (3.18) is equivalent to the one-equation model for the energy conservation with effective properties (Sahraoui & Kaviany 1994; Bubnovich *et al.* 2006). Integrating (3.18) and applying the proper boundary conditions, one finds the first approximation for the temperature profile in the region of thermal equilibrium between the two phases,

$$\theta^{(0)} = \begin{cases} \exp\{(\zeta - \zeta_f)[\varepsilon/(1 - \varepsilon)]\} & \text{for } \zeta \leq \zeta_f, \\ 1 & \text{for } \zeta \geq \zeta_f. \end{cases} \quad (3.19)$$

Note that, since local thermal equilibrium is assumed in this scale, superadiabatic flame temperatures are not possible. This solution is similar to a free-flame solution with the mean properties of an homogeneous medium composed by the gas and the solid phases.

Now, collecting the terms of the order of Γ^{-1} , one finds the equation for the first correction for the temperature as

$$\left(\frac{1 - \varepsilon}{\varepsilon} \right) \frac{d^2\theta^{(1)}}{d\zeta^2} - \frac{d\theta^{(1)}}{d\zeta} = -\frac{d^2\theta^{(0)}}{d\zeta^2}, \quad (3.20)$$

where the condition $\theta_g^{(1)} = \theta_s^{(1)} = \theta^{(1)}$ is still valid.

The boundary conditions for the first correction are $\theta^{(1)} \rightarrow 0$ at $\zeta \rightarrow \pm\infty$ and $\zeta \rightarrow \zeta_f$. Integrating (3.20) with (3.19), the solution for the first correction gives

$$\theta^{(1)} = \begin{cases} -[\varepsilon/(1 - \varepsilon)]^2 (\zeta - \zeta_f) \exp\{[\varepsilon/(1 - \varepsilon)](\zeta - \zeta_f)\} & \text{for } \zeta \leq \zeta_f, \\ 0 & \text{for } \zeta \geq \zeta_f. \end{cases} \quad (3.21)$$

Equations (3.14), (3.17), (3.19) and (3.21) form the type of solution obtained when the one-equation model for the energy conservation is employed to solve the problem of combustion within porous inert media.

3.3. Inner zone: problem of the order of Γ^{-1}

In this thin region, gas and solid phases do not have enough contact time to reach thermal equilibrium. Superadiabatic temperatures are expected to arise, but are limited by the intense interphase heat transfer.

The variation of the non-dimensional variables is of the order of unity along a characteristic length of the order of Γ^{-1} around the flame, except for the solid-phase temperature that presents just a small variation of the order of Γ^{-1} . The variables in this region are denoted by $y_F^{(*)}$, $y_O^{(*)}$, $\theta_s^{(*)}$ and $\theta_g^{(*)}$.

The expansion for the variables can be written as

$$\left. \begin{aligned} y_F^{(*)} &= y_F^{(*)0} + \Gamma^{-1}y_F^{(*)1} + o(\Gamma^{-1}), \\ y_O^{(*)} &= y_O^{(*)0} + \Gamma^{-1}y_O^{(*)1} + o(\Gamma^{-1}), \\ \theta_s^{(*)} &= 1 - \Gamma^{-1}\theta_s^{(*)1} + o(\Gamma^{-1}), \\ \theta_g^{(*)} &= \theta_g^{(*)0} + \Gamma^{-1}\theta_g^{(*)1} + o(\Gamma^{-1}). \end{aligned} \right\} \quad (3.22)$$

Note that the solid-phase temperature has been approximated by unity to leading order. The analysis that justifies $\theta_s^{(*)0} \sim 1$ is presented in Pereira *et al.* (2009). In that work it is shown that as $N \rightarrow \infty$ the solid-phase temperature at the flame θ_{sf} tends to unity, and that θ_{sf} is bounded by $1/2 < \theta_{sf} < 1$. Since l_G represents a thin region around the flame, the solid-phase temperature is assumed equal to unity in the problem to $O(\Gamma^{-1})$. This means that the present model is valid for flames in which the solid-phase temperature at the flame presents a small deviation from the adiabatic limit. With this assumption, the two phases are decoupled at the leading order for this length scale, as will be seen next.

By rescaling the spatial coordinate as $\Gamma(\zeta - \zeta_f) = \xi$, defining $N \equiv N_0\Gamma$, with N_0 being a parameter of the order of unity, substituting the asymptotic expansions (3.22) into the conservation equations (3.6)–(3.9) and collecting the higher-order terms, the governing equations become

$$\varepsilon \frac{dy_F^{(*)0}}{d\xi} = \frac{\varepsilon}{Le_F} \frac{d^2y_F^{(*)0}}{d\xi^2}, \quad (3.23)$$

$$\varepsilon \frac{dy_O^{(*)0}}{d\xi} = \frac{\varepsilon}{Le_O} \frac{d^2y_O^{(*)0}}{d\xi^2}, \quad (3.24)$$

$$\varepsilon \frac{d\theta_g^{(*)0}}{d\xi} = \varepsilon \frac{d^2\theta_g^{(*)0}}{d\xi^2} + N_0(1 - \theta_g^{(*)0}), \quad (3.25)$$

$$0 = (1 - \varepsilon) \frac{d^2\theta_s^{(*)1}}{d\xi^2} - N_0(1 - \theta_g^{(*)0}). \quad (3.26)$$

The boundary conditions are determined when the solution corresponding to the problem of the order of unity is matched with the problem of the order of Γ^{-1} . Thus, in the unburned region, i.e. upstream from the flame, for $\xi \rightarrow -\infty$, $d\theta_g^{(*)}/d\xi$ and $d\theta_s^{(*)}/d\xi$ are equal to $\Gamma^{-1}d\theta^{(0)}/d\zeta$ evaluated at ζ_f . Then, in first approximation, $d\theta_g^{(*)0}/d\xi \sim \Gamma^{-1}\varepsilon/(1 - \varepsilon) \sim 0$ and $d\theta_s^{(*)1}/d\xi \sim -\varepsilon/(1 - \varepsilon)$. Analogously, $y_F^{(*)} = y_O^{(*)} \rightarrow 1$ as $\xi \rightarrow -\infty$. In the burned region, i.e. downstream from the flame, for $\xi \rightarrow \infty$, $\theta_g^{(*)} = \theta_s^{(*)} \rightarrow 1$ and $y_F^{(*)} = y_O^{(*)} - (1 - \phi) = 0$. At the flame, the gas- and solid-phase temperatures, $\theta_{gf}^{(*)}$ and $\theta_{sf}^{(*)}$, are unknowns to be determined.

The solutions of (3.23) and (3.24) are

$$y_F^{(*)0} = \begin{cases} 1 - e^{Le_F(\xi - \xi_f)} & \text{for } \xi \leq \xi_f, \\ 0 & \text{for } \xi \geq \xi_f, \end{cases} \quad (3.27)$$

$$y_O^{(*)0} = \begin{cases} 1 - \phi e^{Le_O(\xi - \xi_f)} & \text{for } \xi \leq \xi_f, \\ 1 - \phi & \text{for } \xi \geq \xi_f. \end{cases} \quad (3.28)$$

Equation (3.25) can be written as

$$\frac{d^2\bar{\theta}}{d\xi^2} - \frac{d\bar{\theta}}{d\xi} - \frac{N_0}{\varepsilon}\bar{\theta} = 0, \quad (3.29)$$

where $\bar{\theta} \equiv (\theta_g^{(*)0} - 1)$. Since $\theta_s^{(*)} = 1$ in a first approximation, (3.29) is independent of the solid-phase temperature and can be integrated. The solution of (3.29) is $\bar{\theta} = C_1 e^{r_1 \xi} + C_2 e^{-r_2 \xi}$. Applying the proper boundary conditions, one finds

$$\theta_g^{(*)0} = \begin{cases} 1 + (\theta_{gf}^{(*)0} - 1)e^{r_1(\xi - \xi_f)} & \text{for } \xi \leq \xi_f, \\ 1 + (\theta_{gf}^{(*)0} - 1)e^{-r_2(\xi - \xi_f)} & \text{for } \xi \geq \xi_f, \end{cases} \quad (3.30)$$

in which $\theta_{gf}^{(*)0}$ is the gas-phase temperature at the flame, yet to be determined, and

$$r_1 = \frac{1}{2} \left[\left(1 + 4 \frac{N_0}{\varepsilon} \right)^{1/2} + 1 \right]$$

and

$$r_2 = \frac{1}{2} \left[\left(1 + 4 \frac{N_0}{\varepsilon} \right)^{1/2} - 1 \right].$$

With knowledge of the leading-order term of the gas solution, $\theta_g^{(*)0}$, (3.26) can be integrated, giving

$$\theta_s^{(*)1} = \begin{cases} \left[(N_0(\theta_{gf}^{(*)0} - 1)) / (r_1^2(1 - \varepsilon)) \right] (e^{r_1(\xi - \xi_f)} - 1) \\ \quad - (\varepsilon / (1 - \varepsilon)) (\xi - \xi_f) + \theta_{sf}^{(*)1} & \text{for } \xi \leq \xi_f, \\ \left[(N_0(\theta_{gf}^{(*)0} - 1)) / (r_2^2(1 - \varepsilon)) \right] (e^{-r_2(\xi - \xi_f)} - 1) \\ \quad + \theta_{sf}^{(*)1} & \text{for } \xi \geq \xi_f. \end{cases} \quad (3.31)$$

Now, applying the continuity of the heat flux in the solid phase at the flame, one finds

$$\theta_{gf}^{(*)0} = 1 + \theta_{sup}, \quad (3.32)$$

$$\theta_{sup} = (1 + N_\varepsilon)^{-1/2}, \quad (3.33)$$

$$N_\varepsilon = 4N_0/\varepsilon. \quad (3.34)$$

Equation (3.32) is the first approximation for the gas-phase temperature at the flame, where θ_{sup} (defined in (3.33)) is the excess temperature at the flame, i.e. the temperature above the adiabatic limit. It is possible to see that θ_{sup} depends only on the parameter N_ε . Then, since $\theta_{sf}^{(*)0} = 1$ as a first approximation, the parameter N_ε , called the porous media flame number, is the parameter that defines universally the leading-order problem at the flame. This result has also been obtained in Pereira *et al.* (2009).

As a way of interpreting the parameter N_ε , an analogy to heat exchange can be made. By using the N_0 and l_G definitions, N_ε can be written as

$$N_\varepsilon = 4 \left(\frac{h_v l_G}{\varepsilon \rho_n S_{FCp}} \right). \quad (3.35)$$

Now, applying the definition of the number of transfer units (NTU) for the heat transfer in a porous medium, we have

$$NTU = \left(\frac{h}{\rho u c_p} \right) \frac{A_{gs}}{A_u} = \left(\frac{h}{\rho u c_p} \right) \frac{S_{gs} V}{\varepsilon A_T} = \frac{h_v L}{\varepsilon \rho u c_p}, \quad (3.36)$$

where h is the surface convection heat transfer coefficient, A_{gs} is the interphase surface area, A_u is the transversal area of the fluid phase, S_{gs} is the interphase surface area density (m^2/m^3) and V , A_T and L are, respectively, the total volume, total transversal area and total length of the porous medium. Then, the parameter N_ε is a particular case of the number of transfer units based on the length scale l_G and on the flame velocity s_F ,

$$N_\varepsilon = 4 NTU_G \quad \text{and} \quad NTU_G = \frac{h_v l_G}{\varepsilon \rho_n s_F c_p}. \quad (3.37)$$

As in heat transfer theory, the number of transfer units denotes the ratio of the axial heat transfer resistance ($1/\rho u c_p A_u$) and the surface heat transfer resistance ($1/h A_{gs}$) (Kaviany 2001). Therefore, a large value of N_ε denotes a small interphase heat transfer resistance when compared to the axial heat transfer resistance at the l_G scale.

Returning to (3.32), it is possible to verify that the superadiabatic effect is more pronounced for lower values of N_ε , i.e. less heat transfer between the phases, and higher values of ε . Equations (3.32)–(3.34) show that, in a first approximation, the flame temperature does not depend on the solid conductivity. This happens because the solid-phase temperature is unity in a first approximation. Therefore, under the conditions considered in this analysis ($N \sim \Gamma \gg 1$), the interphase heat transfer is the limiting process that defines the flame properties.

Applying the remaining boundary condition, one finds

$$\theta_{sf}^{(*) (1)} = \frac{N_0 (\theta_{gf}^{(*) (0)} - 1)}{r_2^2 (1 - \varepsilon)} = \left(\frac{\varepsilon}{1 - \varepsilon} \right) \frac{\theta_{sup} (1 + \theta_{sup})}{(1 - \theta_{sup})}, \quad (3.38)$$

which is the first correction for the solid-phase temperature at the flame.

Now, collecting the terms of the order of Γ^{-1} for the gas phase, one finds

$$\varepsilon \frac{d\theta_g^{(*) (1)}}{d\xi} = \varepsilon \frac{d^2 \theta_g^{(*) (1)}}{d\xi^2} - N_0 (\theta_s^{(*) (1)} + \theta_g^{(*) (1)}), \quad (3.39)$$

where the boundary conditions are $d\theta_g^{(*) (1)}/d\xi = \varepsilon/(1 - \varepsilon)$ for $\xi \rightarrow -\infty$ and $\theta_g^{(*) (1)} = 0$ for $\xi \rightarrow \xi_f$. Then, the first correction of gas-phase temperature, for $\xi \leq \xi_f$, can be determined as (see Appendix A)

$$\theta_g^{(*) (1)} = \frac{\varepsilon}{1 - \varepsilon} \left[\frac{-15(\theta_{sup}^2 - 1/5)(\theta_{sup}^2 + 1/3)}{4\theta_{sup}^2 (1 - \theta_{sup}^2)} (1 - e^{r_1(\xi - \xi_f)}) + (\xi - \xi_f) \right]. \quad (3.40)$$

Although the present model does not describe either the limit $N_\varepsilon \rightarrow 0$ or the limit $N_\varepsilon \rightarrow \infty$, the analysis of these limits is able to reveal qualitatively the results from Pereira *et al.* (2009) and information of the flame extinction, respectively. For the conditions such that $\theta_{sup} \rightarrow 1$ ($N_\varepsilon \rightarrow 0$) according to (3.33), the term multiplying the exponential term in (3.40) goes to minus infinity, showing that the flame temperature $\theta_{gf}^{(*)}$ satisfies $(2 - \theta_{gf}^{(*)}) \gg \Gamma^{-1}$, as pointed out by (3.22), (3.32) and (3.40). However, for the conditions such that $\theta_{sup} \rightarrow 0$ ($N_\varepsilon \rightarrow \infty$), according to (3.33), the term multiplying the exponential term in (3.40) goes to infinity, showing that the flame temperature $\theta_{gf}^{(*)}$

satisfies $(\theta_{gf}^{(*)} - 1) \gg \Gamma^{-1}$. This result shows that superadiabatic flame temperatures are observed even for large values of N_ε , agreeing with the necessary conditions for the flame propagation that will be found in the next section.

3.4. Inner zone: reaction region $O(\delta\Gamma^{-1})$

In a region of the order of $\delta\Gamma^{-1}$ around the flame, the variables present a variation of the order of δ . The solution follows the same steps already discussed in Pereira *et al.* (2009) for higher equivalence ratios.

The expression relating the flame velocity with the problem parameters is

$$s_F^2 = \frac{2A\rho_f^2\lambda_g Y_{O_n} T_{gf}^a \exp(-\beta/\alpha)}{(\rho_n^2 c_p)} [\delta^2 Le_F (1 - \phi)] \exp \left\{ \frac{-\beta(1 - \theta_{gf}^{(*)})}{1 - \alpha(1 - \theta_{gf}^{(*)})} + m n \right\}, \quad (3.41)$$

in which

$$\delta = [1 + \alpha(\theta_{gf}^{(*)} - 1)]^2 / \beta.$$

In (3.41) the parameter n is a displacement in the coordinate axis in order to match the solution in the reaction length scale l_R with the solution in the gas-phase diffusion length scale l_G . The parameter m represents the ratio of the thermal flux downstream from the flame to the total heat release. Liñán (1974) proposed an approximate expression for a curve fit of the numerical solution of the problem in the reaction region, relating these two parameters by

$$m n = 1.344m - 4m^2(1 - m)/(1 - 2m) + 3m^3 - \ln(1 - 4m^2) \quad \text{for } 0 < m < 0.5. \quad (3.42)$$

The value of m can be determined from the gas temperature profile (3.30), resulting in

$$m = r_2/(r_1 + r_2) = (1 - \theta_{sup})/2. \quad (3.43)$$

As already discussed in the previous work, for combustion within porous media the value of m is bounded by $0 \leq m \leq 1/2$. The limit $m = 0$ corresponds to a freely propagating flame with no heat loss downstream from the flame, while the excess of enthalpy requires $m > 0$. The limit $m \rightarrow 1/2$ corresponds to a situation in which the heat loss downstream from the flame is equal to the heat loss upstream from the flame, and under this condition the flame is not stable, i.e. there is extinction. Then, the flame temperature needs to be above the adiabatic free-flame temperature for the flame propagation to be possible, i.e. $\theta_{sup} > 0$.

3.5. Model summary

A closed-form approximated solution for the structure and propagation velocity of ultra-lean adiabatic stationary premixed flames in porous inert media is obtained. The temperature profile of both phases for the region of thermal equilibrium is given by (3.14), (3.17), (3.19) and (3.21). In the region of thermal non-equilibrium, the temperature profile of the gas phase is described by (3.22), (3.30), (3.32) and (3.40) and the temperature profile of the solid phase is described by (3.22), (3.31), (3.32) and (3.38). The fuel and oxidant mass fraction profiles are given by (3.27) and (3.28). The flame velocity is evaluated by (3.41), in which (3.42) and (3.43) are used.

This set of equations is able to qualitatively predict, under the limitations imposed by the simplifying assumptions, the main characteristics of flames in porous media for heat transfer parameters N of the order of Γ . A condition imposed in this solution is $\varepsilon/(1 - \varepsilon) \sim O(1)$, which ensures the separation of the length scales of the problem.

Properties and parameters			Results		
R_u	8.314	J (mol K) ⁻¹	λ_s	4.041	W (m K) ⁻¹
E_a	1.2×10^5	J mol ⁻¹	h_v	1.476×10^4	W (m ³ K) ⁻¹
A	1.0×10^{10}	m ³ (kg s) ⁻¹	T_r	838	K
a	0		$T_{g,f}$	1052.1	K
Q	4.759×10^7	J kg ⁻¹	$T_{s,f}$	805.0	K
c_p	1141	J (kg K) ⁻¹	s_F	2.252	cm s ⁻¹
λ_g	0.0673	W (m K) ⁻¹	N_0	1.072	
ρ_n	1.185	kg m ⁻³	$lpha$	0.64	
T_n	298	K	β	11.1	
C'	0.146		Da_f	42.74	
m'	0.83		\overline{Da}_f	0.37	
ε	0.8		m	0.3017	
ϕ	0.225		n	0.9926	
φ	50	p.p.i.	δ	0.142	
Γ	60		N	64.31	
Le_F	1		$\theta_{g,f}$	1.397	

TABLE 1. Properties and parameters used in the calculations and results for $\phi = 0.225$, $\Gamma = 60$, $\varepsilon = 0.8$, $\varphi = 50$ p.p.i. and $Le_F = 1$.

The model is also restricted to the conditions where the solid-phase temperature at the flame presents small deviations from the adiabatic limit. In the next section the model will be explored to evaluate the influence of the problem parameters on such flames.

4. Discussion

For the results that follow, the reaction rate parameters were adjusted to agree with measured laminar methane–air flame speeds for free flames with equivalence ratios ranging from 0.5 to 0.6 (Zhu, Egolfopoulos & Law 1989). The heat of reaction was adjusted to reproduce the adiabatic flame temperature for $\phi = 0.5$. The gas-phase properties were approximated by the air properties evaluated at 1000 K. The volumetric heat transfer coefficient h_v is modelled following Fu, Viskanta & Gore (1998), which uses a volumetric Nusselt number, $Nu_v = C' Re^{m'}$, where $Nu_v = h_v l_d^2 / \lambda_g$ and Re is the Reynolds number, $Re = \rho_n u_n l_d / \mu_n$, where μ_n is the gas-phase viscosity. The parameters C' and m' are curve-fitting constants. The mean pore diameter is modelled as $l_d = (\sqrt{4\varepsilon/\pi}) / (39.37\varphi)$, which is a uniform pore distribution model, where φ is the linear pore density given in pores per inch (p.p.i.). Note that the variations of h_v are expressive for extremely lean mixtures and the present analysis must take this variation into account. The used transport and geometric properties of the solid phase are typical of porous burners (Möbbauer *et al.* 1999; Catapan, Pereira & Oliveira 2005). Table 1 shows the parameters and properties used in the calculations and some of the results obtained.

4.1. Influence of the equivalence ratio

Figure 2 shows the flame velocity s_F as a function of equivalence ratio ϕ . The upper branch of the curve corresponds to a physical solution while the lower branch corresponds to a non-physical solution ($N \gg \Gamma$). Below $\phi = 0.217$, the parameter m approaches the limiting value 0.5 and the steady-state flame propagation is not possible. Then, the present model predicts a flammability limit for the premixed

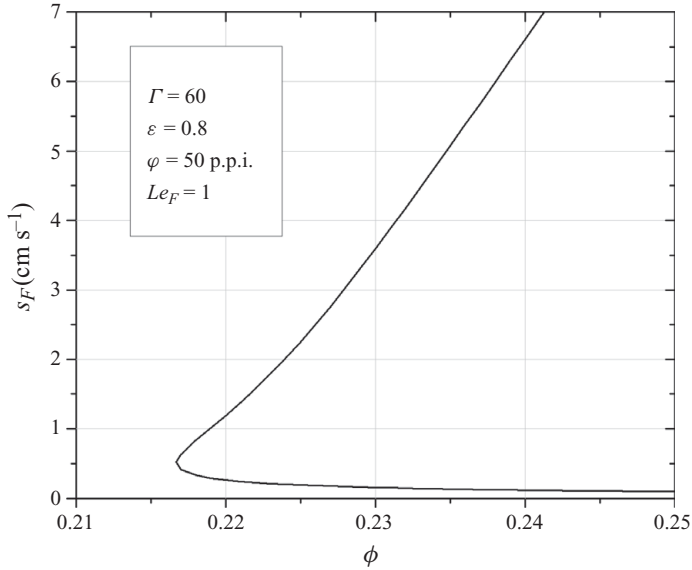


FIGURE 2. The flame velocity s_F as a function of the equivalence ratio ϕ . The upper branch corresponds to the physical solution.

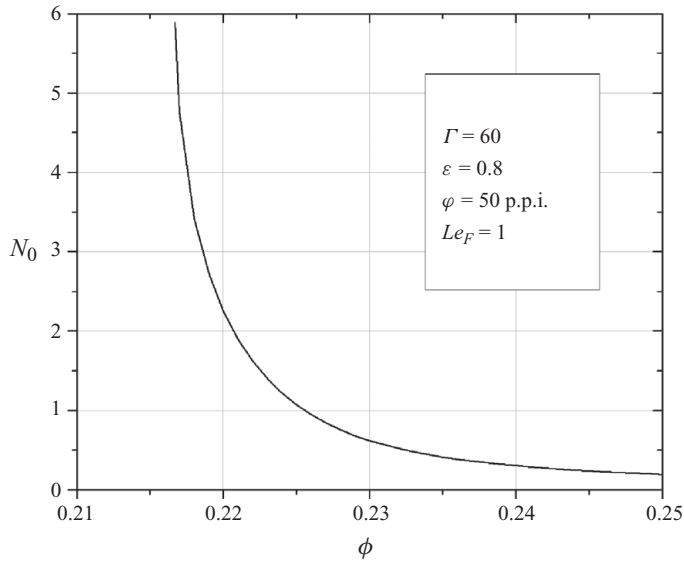


FIGURE 3. The parameter N_0 as a function of ϕ .

methane–air combustion within porous inert media. For the porous medium under analysis, this limit is found around $\phi = 0.217$, while for free methane–air flames, this limit is found around $\phi = 0.5$. All the subsequent analysis will be restricted to the physical branch of the solution.

Figure 3 shows the parameter $N_0 = N/\Gamma$ as a function of the equivalence ratio ϕ . The model is constructed for $N_0 \sim O(1)$, so we see that the solution is valid for a small range of equivalence ratios around $\phi = 0.225$. Since N_0 is proportional to $1/s_F^2$,

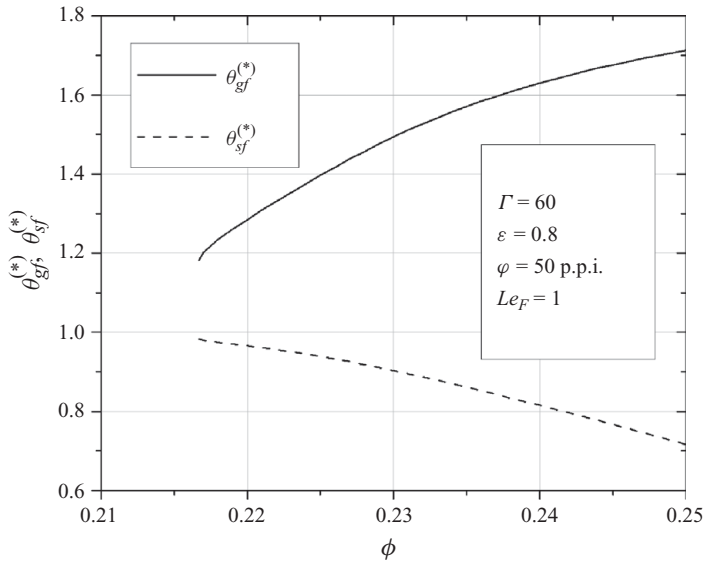


FIGURE 4. Gas- and solid-phase temperatures at the flame as a function of ϕ .

for leaner mixtures the corresponding lower flame velocities result in higher values of N_0 .

Figure 4 shows the gas- and solid-phase temperatures at the flame as a function of the equivalence ratio ϕ . Contrary to the previous model, where the condition $N \sim O(1)$ was considered, for the condition $N \sim O(\Gamma)$, the non-dimensional flame temperature, $\theta_{gf}^{(*)}$, increases as ϕ is increased. This is a consequence of (3.32)–(3.34), in which $\theta_{gf}^{(*) (0)}$ varies with $N_0^{-1/2}$. Physically, the reason for this behaviour is the intense heat transfer from the gas phase to the solid phase that occurs at the gas-phase diffusion length scale for leaner mixtures. Lower values of ϕ result in lower flame velocities; thus there is more time for the interphase heat transfer and the gas-phase temperature is limited by the intense heat loss to the solid matrix. As ϕ is further decreased, there is a point at which the temperatures at the flame are not high enough to sustain the flame and a flammability limit is found. As the superadiabatic flame temperature decreases, i.e. as θ_{sup} decreases, the heat flux to the downstream side of the flame becomes more important and the parameter m tends to the limiting value of $1/2$, according to (3.43). Then, one can conclude that, to sustain flames at ϕ smaller than the free-flame flammability limit, it is necessary to reach a minimum superadiabatic flame temperature, i.e. $\theta_{sup} > 0$, as discussed in relation to (3.43). For the conditions considered in figure 4, the temperature at the flame must be at least 20% above the adiabatic free-flame temperature.

It is interesting to note that for moderately lean mixtures the non-dimensional superadiabatic flame temperature increases when ϕ is decreased (Pereira *et al.* 2009), whereas for the ultra-lean mixtures the opposite is observed. Then, we expect to find a point of maximum non-dimensional superadiabatic flame temperature in the lean side of the equivalence ratio range. This can be understood by considering the two limiting cases presented in §2. For $N \rightarrow 0$ the two equations for the conservation of energy are decoupled and the flame structure has the same structure of a free flame. The solid phase plays no role in the solution and superadiabatic flame temperatures are not possible. For $N \rightarrow \infty$ the two phases are in local thermal equilibrium and

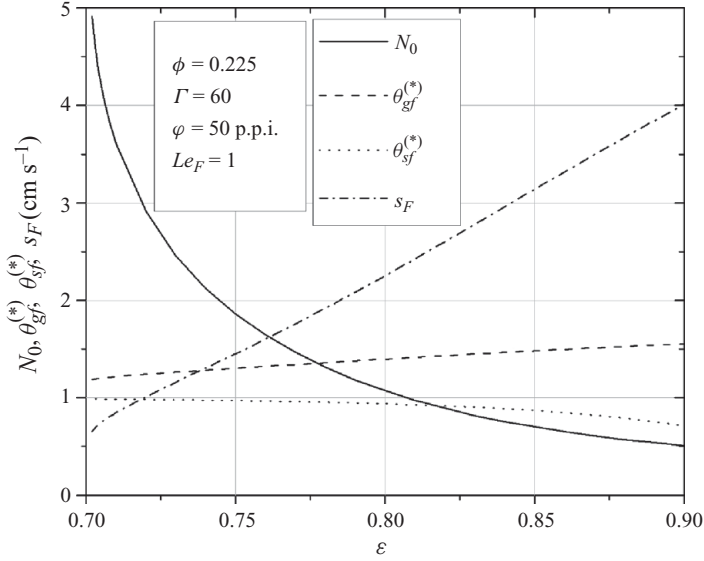


FIGURE 5. Dependence of N_0 , $\theta_{gf}^{(*)}$, $\theta_{sf}^{(*)}$ and s_F on ε .

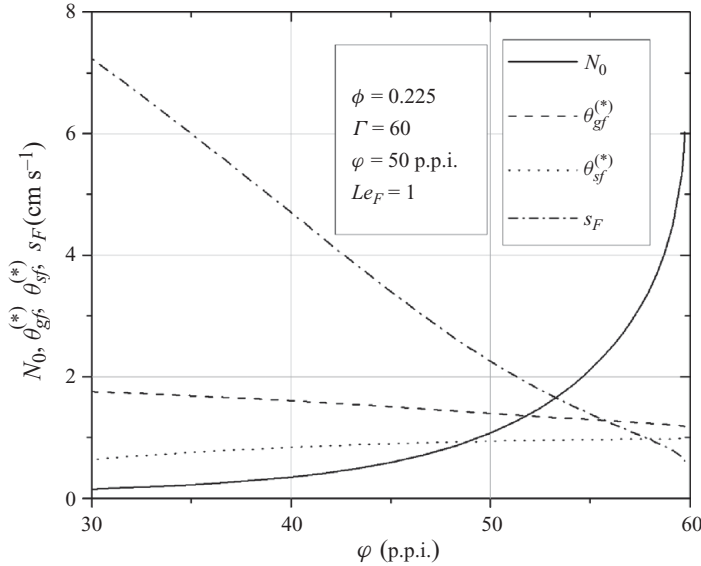
the problem reduces to a one-equation model, i.e. a free-flame-like structure for an homogeneous medium with effective properties, and again superadiabatic flame temperatures are not possible. For intermediate values of N thermal non-equilibrium between the phases and superadiabatic flame temperatures are found and a point of maximum non-dimensional superadiabatic flame temperature must exist.

An interesting characteristic of the model is that (3.32) and (3.38) do not depend on Γ , i.e. in a first approximation the solid thermal conductivity λ_s does not influence the gas- and solid-phase temperature at the flame. This happens because, with the approximation $\theta_s^{(*) (0)} = 1$, the heat conduction in the solid phase is not the limiting process for the gas-phase preheating. Instead, the interphase heat transfer and the convective–diffusive balance in the gas phase are the controlling processes that define the properties at the flame. Nevertheless, the solid-phase conductivity impacts the extension of the flame thickness l_s . For ultra-lean mixtures, the solid-phase diffusion length scale is very large. For example, the flame thickness reaches 20 cm for $\phi = 0.225$, $\Gamma = 60$, $\varepsilon = 0.8$ and $\varphi = 50$ p.p.i. This occurs because the low flame velocities of these extremely lean mixtures allow a wide thermal penetration.

According to (3.22), the solid-phase temperature at the flame is found by $\theta_{sf}^{(*)} = 1 - \Gamma^{-1} \theta_{sf}^{(*) (1)}$. According to (3.38), $\theta_{sf}^{(*) (1)}$ varies with $N_0^{-1/2}$, and since N_0 increases as ϕ decreases, the solid-phase temperature at the flame $\theta_{sf}^{(*)}$ is expected to increase for lower values of ϕ . This is a consequence of the intense interphase heat transfer found in extremely lean mixtures. As N_0 increases, the solid- and gas-phase temperatures at the flame becomes closer, approaching the adiabatic limit, i.e. $\theta_{gf}^{(*)} \rightarrow 1$ and $\theta_{sf}^{(*)} \rightarrow 1$.

4.2. Influence of the matrix properties

Figure 5 shows the dependence of the interphase heat transfer parameter N_0 , the flame temperature $\theta_{gf}^{(*)}$, the solid-phase temperature at the flame $\theta_{sf}^{(*)}$ and the flame velocity s_F on the porosity ε . The effect of decreasing ε , for a constant ϕ , is to decrease the mean pore diameter l_d , thus resulting in a large heat transfer coefficient h_v and, consequently, in a large value of N_0 . Again, the effect of increasing N_0 is to decrease


 FIGURE 6. Dependence of N_0 , $\theta_{gf}^{(*)}$, $\theta_{sf}^{(*)}$ and s_F on ϕ .

the superadiabatic effect. According to (3.32)–(3.34), the gas-phase temperature at the flame varies as $\varepsilon^{1/2}$. The flame velocity follows the gas-phase temperature at the flame and increases with increasing values of ε . As N_0 increases the solid-phase temperature at the flame approaches the limiting value of unity.

When the linear density of pores ϕ is increased while maintaining a constant porosity ε , the mean pore diameter decreases. This leads to a solid matrix with a large specific superficial area (m^2/m^3), thus increasing the interphase heat transfer coefficient h_v and the parameter N_0 . The behaviour of the flame variables when increasing ϕ is shown in figure 6 and is similar to that of decreasing the porosity, i.e. for higher values of N_0 the superadiabatic effect decreases.

It is interesting to note that, decreasing ϕ , the condition $N_0 \sim O(1)$ is obtained for decreasing values of ϕ , i.e. the decrease in h_v caused by the larger pores has to be balanced by the lower flame velocities obtained for leaner mixtures. This, in turn, leads to decreasing values for the lean flammability limit, as shown in figure 7. This result shows that, for premixed combustion within porous inert media, the lean flammability limit is no longer a property of the reactants mixtures only, but it also depends on the solid matrix properties. Additionally, at the lean flammability limit, the reaction length scale l_R is of the order of the pore diameter l_d , showing that, in this limit, the interphase heat transfer tends to be important even at the innermost length scale.

It is important to recall that, although the present model is based on the one-step reaction mechanism, this approximation is adequate for this first theoretical approach since it permits the adjustment of a few chemical parameters to agree with experiments. Despite this and other simplifying assumptions, the results reveal the strong dependence of the flammability limit for premixed flames in porous inert media on the matrix properties. To improve this prediction, more complex mechanisms should be considered and experiments should be carried out to correctly determine the volumetric interphase heat transfer coefficient h_v at the flow rates and temperatures of interest. Additionally, since the value of N_0 is much higher than one

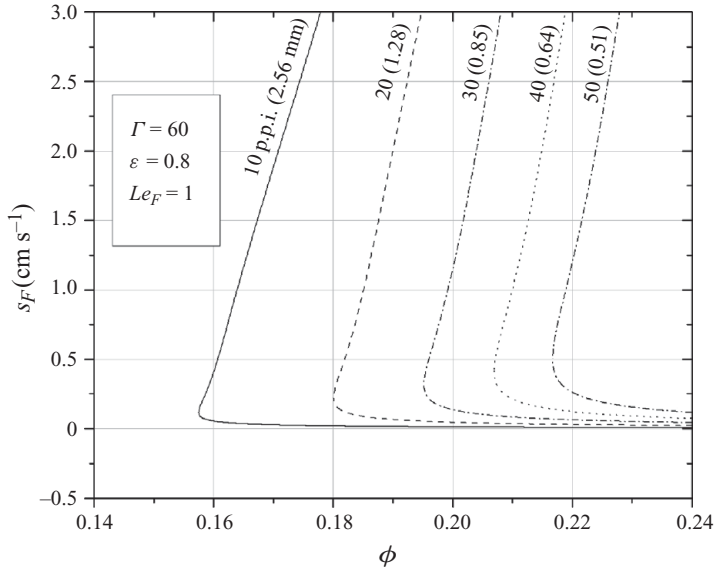


FIGURE 7. The flame velocity s_F as function of ϕ for different values of ϕ . The numbers in parenthesis for each curve are the corresponding mean pore diameters.

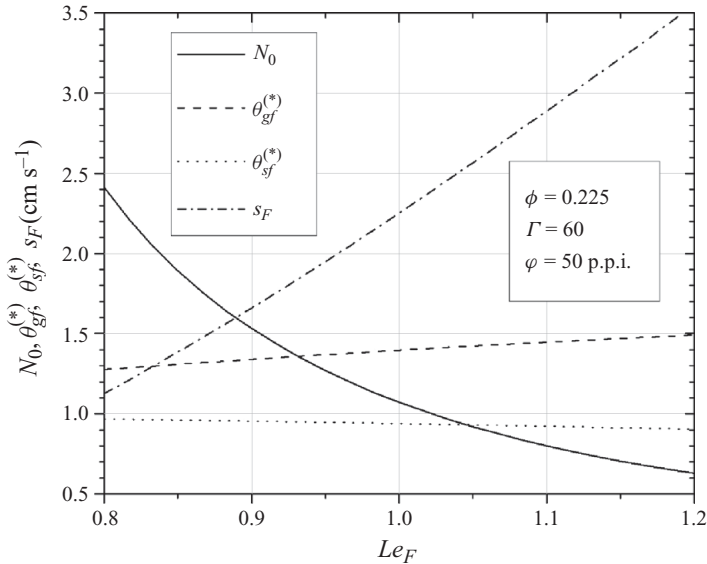


FIGURE 8. Dependence of N_0 , $\theta_{gf}^{(*)}$, $\theta_{sf}^{(*)}$ and s_F on Le_F .

in the flammability limit, the precise determination of this limit requires a model considering the condition $N \gg \Gamma$.

4.3. Influence of the Lewis number

Figure 8 shows the effect of fuel Lewis number Le_F on the flame variables. Since, according to (3.41), lower flame velocities s_F are found for lower values of Le_F , the interphase heat transfer is intensified when Le_F is decreased due to the longer contact time between the phases and, consequently, the superadiabatic effect is also decreased.

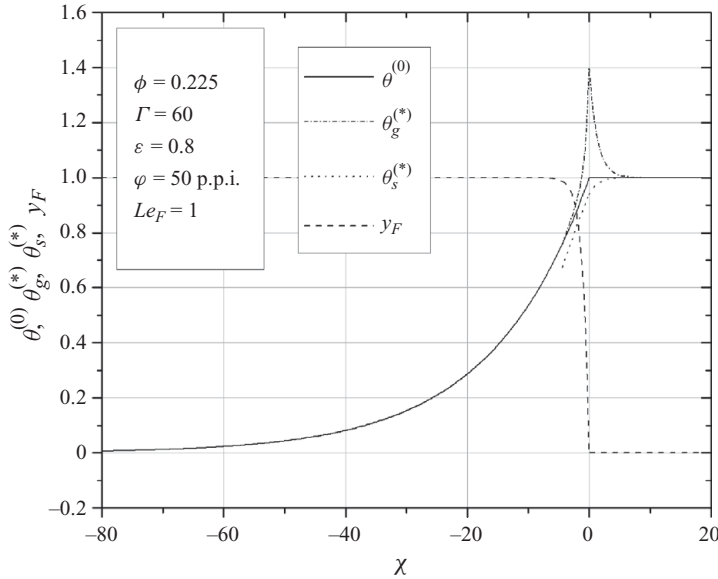


FIGURE 9. Flame structure for $\phi = 0.225$, $\Gamma = 60$, $\varepsilon = 0.8$, $\varphi = 50$ p.p.i. and $Le_F = 1$.

This behaviour is contrary to that found for higher equivalent ratio, as shown in a previous work (Pereira *et al.* 2009).

4.4. Flame structure

Figure 9 shows the flame structure for $\phi = 0.225$, $\Gamma = 60$, $\varepsilon = 0.8$, $\varphi = 50$ p.p.i. and $Le_F = 1$. The gas- and solid-phase temperatures obtained for the problems of $O(1)$ and $O(\Gamma^{-1})$ are presented. A composite solution would be necessary to obtain uniformly valid expressions for the temperature profiles. Nevertheless, as shown in Appendix B, this would require the solution of additional terms for the asymptotic expansions that do not bring new information to the problem.

The present solution shows that, even though we are dealing with a problem that presents local thermal equilibrium in a wide region around the flame, the choice to model the problem with the one-equation model for the conservation of energy would neglect the existence of superadiabatic flame temperatures in a thin region around the flame. These superadiabatic flame temperatures decrease as the interphase heat transfer is increased; however, there should exist a small region of thermal non-equilibrium around the flame where superadiabatic flame temperatures will be found, in order for the flame to be sustained. This result cannot be obtained with the models that assume local thermal equilibrium between the phases over the entire domain of solution.

5. Conclusions

An analysis of adiabatic stationary planar premixed flames within inert porous media is proposed for the conditions of $N \sim O(\Gamma)$ and $\varepsilon/(1-\varepsilon) \sim O(1)$. The condition $N \sim O(\Gamma)$ is characterized by an intense interphase heat transfer that can be found for extremely lean mixtures or for solid matrices with very small pore sizes. These flames present a wide region of local thermal equilibrium between the phases and the superadiabatic effect is limited by the intense interphase heat transfer at the gas-phase diffusion length scale l_G .

The superadiabatic effect is less pronounced for lower values of ε and higher values of φ . This behaviour is related to the increase in the interphase heat transfer coefficient h_v . The superadiabatic effect is also less pronounced for lower values of Le_F , a behaviour which is connected to the lower flame velocities observed for decreasing values of Le_F .

The analysis shows that the superadiabatic flame temperature decreases as ϕ is decreased, i.e. as the interphase heat transfer becomes more intense. Since, in a previous model, valid for higher equivalence ratios, the superadiabatic flame temperature increases when ϕ is decreased, a maximum non-dimensional superadiabatic flame temperature in the lean side of the equivalence ratio range is expected to exist.

For extremely lean mixtures, the gas-phase temperature at the flame must reach a minimum superadiabatic flame temperature for the flame propagation to be possible. Thus, the model shows the existence of a flammability limit for ultra-lean mixtures. For methane–air flames, considering $Le_F = 1$, and with $\Gamma = 60$, $\varepsilon = 0.8$ and $\varphi = 50$ p.p.i., the present analysis predicts the lean flammability limit to ‘occur’ around $\phi = 0.217$ with a gas-phase temperature at the flame 20% above the adiabatic limit. A better determination of this limit would require the use of more complex kinetic mechanisms and the solution of the problem of $N_0 \gg 1$. These results cannot be obtained with the models that assume local thermal equilibrium between the phases over the entire domain of solution because these models do not allow superadiabatic flame temperatures to arise.

The authors gratefully acknowledge the Programa de Pós-Graduação em Engenharia Mecânica da UFSC (POSMEC) and the ANP PRH-09 (MECPETRO) for financial support for the development of this work. The third author acknowledges CAPES (GRANT PNPD) and CNPq (GRANT 563835/2008-7 552417/2009-2) for partial financial support.

Appendix A. First correction for the gas-phase temperature for the problem of the order of Γ^{-1}

The first correction for the gas-phase temperature for the problem of the order of Γ^{-1} is important for $\xi \leq \xi_f$, since the boundary condition at $\xi \rightarrow -\infty$ was not used in the leading-order solution. Then, combining (3.39) with (3.31) for $\xi \leq \xi_f$ one arrives at the following heterogeneous second-order differential equation:

$$\frac{d^2\theta_g^{(*)1}}{d\xi^2} - \frac{d\theta_g^{(*)1}}{d\xi} - \frac{N_0}{\varepsilon}\theta_g^{(*)1} = \frac{N_0}{\varepsilon} \left\{ \theta_{sf}^{(*)1} \left[1 + \left(\frac{r_2}{r_1}\right)^2 \left(e^{r_1(\xi-\xi_f)} - 1 \right) \right] - \frac{\varepsilon}{1-\varepsilon}(\xi - \xi_f) \right\}. \quad (\text{A } 1)$$

The solution of (A1) is the sum of the solution of the respective homogeneous equation with the solution of the particular case. The homogeneous equation has a solution of the form

$$\theta_{g,h}^{(*)1} = C_1 e^{r_1 \xi} - C_2 e^{r_2 \xi}, \quad (\text{A } 2)$$

where C_1 and C_2 are constants to be determined by applying the boundary conditions. The particular solution is

$$\theta_{g,p}^{(*)1} = C_3 e^{r_1 \xi} + C_4 \xi + C_5, \quad (\text{A } 3)$$

where the constants are

$$C_3 = \frac{\theta_{sf}^{(*)}(1) (r_2/r_1)^2 N_0/\varepsilon}{r_1^2 - r_1 - N_0/\varepsilon}, \quad C_4 = \frac{\varepsilon}{1 - \varepsilon}, \quad C_5 = \theta_{sf}^{(*)}(1) \left[\left(\frac{r_2}{r_1} \right)^2 - 1 \right] + \frac{N_0}{1 - \varepsilon}.$$

Then, the solution of (A 1) is

$$\theta_g^{(*)}(1) = (C_1 + C_3) e^{r_1 \xi} - C_2 e^{r_2 \xi} + C_4 \xi + C_5, \tag{A 4}$$

with the boundary conditions $d\theta_g^{(*)}(1)/d\xi = \varepsilon/(1 - \varepsilon)$ for $\xi \rightarrow -\infty$ and $\theta_g^{(*)}(1) = 0$ for $\xi = \xi_f$. Then, the constants C_1 and C_2 can be determined from (A 4) and one arrives at

$$\theta_g^{(*)}(1) = \left\{ \theta_{sf}^{(*)}(1) \left[\left(\frac{r_2}{r_1} \right)^2 - 1 \right] + \frac{N_0}{1 - \varepsilon} \right\} (1 - e^{r_1(\xi - \xi_f)}) + \left(\frac{\varepsilon}{1 - \varepsilon} \right) (\xi - \xi_f). \tag{A 5}$$

Now, substituting the expressions for $\theta_{sf}^{(*)}(1)$, r_1 and r_2 into (A 5), (3.40) is recovered.

Appendix B. Composite solutions

Uniformly valid solutions for the gas- and solid-phase temperatures, without gaps or spurious corners, can be obtained by constructing a composite solution. This is done by summing the respective inner, $O(\Gamma^{-1})$, and outer, $O(1)$, solutions and then subtracting the terms common to both solutions.

For the solid phase, for example, to find the common terms, the outer solution, given by (3.14), is rewritten in terms of the inner variable ξ , and the limit $\Gamma \rightarrow \infty$ is taken, i.e. the inner limit of the outer solution is found. To order Γ^{-1} , the terms common to both solutions are found to be $1 + \Gamma^{-1}[\varepsilon/(1 - \varepsilon)]\xi$. Then, a composite solution can be written as

$$\theta_{s,c} = \begin{cases} \exp [\Gamma^{-1} (\varepsilon/(1 - \varepsilon)) \xi] \\ -\Gamma^{-1} \theta_{sf}^{(*)}(1) [1 + (r_1/r_2)^2 (e^{r_1 \xi} - 1)] & \text{for } \xi \leq \xi_f, \\ 1 - \Gamma^{-1} \theta_{sf}^{(*)}(1) e^{-r_2 \xi}, & \text{for } \xi \geq \xi_f. \end{cases} \tag{B 1}$$

The problem with (B 1) is that it does not recover the boundary condition at $\xi \rightarrow -\infty$. In the present problem, the correct limits as $\xi \rightarrow -\infty$ for the composite solutions of the solid- and gas-phase temperatures are asymptotically reached as additional terms are included in the respective inner and outer solutions. However, since these additional terms are not relevant to the conclusions of the present work, they will not be solved.

REFERENCES

BOSHOFF-MOSTERT, L. & VILJOEN, H. J. 1996 Analysis of the homogeneous combustion in monolith structures. *Chem. Engng Sci.* **51**, 1107–1111.

BUBNOVICH, V. I., ZHDANOK, S. A. & DOBREGO, K. V. 2006 Analytical study of the combustion waves propagation under filtration of methane–air mixture in a packed bed. *Intl J. Heat Mass Transfer* **49**, 2578–2586.

BUCKMASTER, J. D. & TAKENO, T. 1981 Blow-off and flashback of an excess-enthalpy flame. *Combust. Sci. Technol.* **25**, 153–159.

CATAPAN, R. C., PEREIRA, F. M. & OLIVEIRA, A. A. M. 2005 Development of a radiant porous burner with a combined thermal and fluidynamic mechanism of flame stabilization. In *Proceedings of the International Congress of Mechanical Engineering: COBEM 2005* Ouro Preto, MG, Brazil.

- DESHAIES, B. & JOULIN, G. 1980 Asymptotic study of an excess-enthalpy flame. *Combust. Sci. Technol.* **22**, 281–285.
- DOBREGO, K. V., GNESDILOV, N. N., LEE, S. H. & CHOI, H. K. 2008 Lean combustibility limit of methane in reciprocal flow filtration combustion reactor. *Intl J. Heat Mass Transfer* **51**, 2190–2198.
- ECHIGO, R. 1991 Radiation enhanced/controlled phenomena of heat and mass transfer in porous media. *ASME/JSME Therm. Engng Proc.* **4**, 21–32.
- FACHINI, F. F. 1996 The effects of the acoustic field on droplet extinction processes. *Combust. Sci. Technol.* **156**, 237–253.
- FACHINI, F. F. 2005 Large-activation-energy asymptotic analysis of multicomponent fuel diffusion flames. *Combust. Sci. Technol.* **177**, 1793–1811.
- FACHINI, F. F., LIÑÁN, A. & WILLIAMS, F. A. 1999 Theory of flame histories in droplet combustion at small stoichiometric fuel-air ratios. *AIAA J.* **37**, 1426–1435.
- FU, X., VISKANTA, R. & GORE, J. P. 1998 Measurement and correlation of volumetric heat transfer coefficients of cellular ceramics. *Exp. Therm. Fluid Sci.* **17**, 285–293.
- GOLOMBOK, M., PROTHERO, A., SHIRVILL, L. C. & SMALL, L. M. 1991 Surface combustion in metal fibre burners. *Combust. Sci. Technol.* **77**, 203–223.
- HACKERT, C. L., ELLZEY, J. L. & EZEKOYE, O. A. 1999 Combustion and heat transfer in model two-dimensional porous burners. *Combust. Flame* **116**, 177–191.
- HARDESTY, D. R. & WEINBERG, F. J. 1974 Burners producing large excess enthalpies. *Combust. Sci. Technol.* **8**, 201–214.
- HENNEKE, M. R. & ELLZEY, J. 1999 Modeling of filtration combustion in a packed bed. *Combust. Flame* **117**, 832–840.
- HOFFMANN, J. G., ECHIGO, R., YOSHIDA, H. & TADA, S. 1997 Experimental study on combustion in porous media with a reciprocating flow system. *Combust. Flame* **111**, 32–46.
- HOWELL, J. R., HALL, M. J. & ELLZEY, J. L. 1996 Combustion of hydrocarbon fuels within porous inert media. *Prog. Energy Combust. Sci.* **22**, 121–145.
- HSU, P., EVANS, W. D. & HOWELL, J. R. 1993 Experimental and numerical study of premixed combustion within nonhomogeneous porous ceramics. *Combust. Sci. Technol.* **90**, 149–172.
- KAVIANY, M. 1995 *Principles of Heat Transfer in Porous Media*, 2nd edn. Springer.
- KAVIANY, M. 2001 *Principles of Heat Transfer*. Wiley.
- KOTANI, Y., BEHBAHANI, H. F. & TAKENO, T. 1984 An excess enthalpy flame combustor for extended flow ranges. In *Proceedings of 20th Symposium (Int.) on Combustion*, pp. 2025–2033.
- KOTANI, Y. & TAKENO, T. 1982 An experimental study on stability and combustion characteristics of an excess enthalpy flame. In *Proceedings of 19th Symposium (Int.) on Combustion*, pp. 1503–1509.
- LAW, C. K. 2006 *Combustion Physics*. Cambridge University Press.
- LIÑÁN, A. 1974 The asymptotic structure of counterflow diffusion flames for large activation energies. *Acta Astronaut.* **1**, 1007–1039.
- LIU, J. F. & HSIEH, W. H. 2004 Experimental investigation of combustion in porous heating burners. *Combust. Flame* **138**, 295–303.
- MCINTOSH, A. C. 1988 Simplified model of a surface-combustion burner with radiant heat emission. *AIAA Prog. Astronaut. Aeronaut.* **113**, 385–405.
- MCINTOSH, A. C. & PROTHERO, A. 1991 A model of large heat transfer surface combustion with radiant heat emission. *Combust. Flame* **83**, 111–126.
- MIN, D. K. & SHIN, H. D. 1991 Laminar premixed flame stabilized inside a honeycomb ceramic. *Intl J. Heat Mass Transfer* **34**, 341–356.
- MÖBBAUER, S., PICKENÄCKER, O., PICKENÄCKER, K. & TRIMIS, D. 1999 Application of the porous burner technology in energy- and heat-engineering. In *Proceedings of the Fifth International Conference on Technologies and Combustion for a Clean Environment (Clean Air V)*, Lisbon, Portugal, vol. 1, pp. 519–523.
- OLIVEIRA, A. A. M. & KAVIANY, M. 2001 Nonequilibrium in the transport of heat and reactants in combustion in porous media. *Prog. Energy Combust. Sci.* **27**, 523–545.
- PEREIRA, F. M., OLIVEIRA, A. A. M. & FACHINI, F. F. 2009 Asymptotic analysis of stationary adiabatic premixed flames in porous inert media. *Combust. Flame* **156**, 152–165.
- SAHRAOUI, M. & KAVIANY, M. 1994 Direct simulation vs. volume-averaged treatment of adiabatic, premixed flame in a porous medium. *Intl J. Heat Mass Transfer* **37**, 2817–2834.

- SCHOEGL, I. & ELLZEY, J. 2007 Superadiabatic combustion in conducting tubes and heat exchangers of finite length. *Combust. Flame* **151**, 142–159.
- SCHULTZ, D. A., MATKOWSKY, B. J., VOLKER, V. A. & FERNANDEZ-PELLO, A. C. 1996 Forced forward smolder combustion. *Combust. Flame* **104**, 1–26.
- SHI, J. R., XIE, M. Z., LIU, H., LI, G. & ZHOU, L. 2008 Numerical simulation and theoretical analysis of premixed low-velocity filtration combustion. *Intl J. Heat Mass Transfer* **51**, 1818–1829.
- TELENGATOR, A. M., WILLIAMS, F. A. & MARGOLIS, S. B. 2006 Finite-rate interphase heat transfer effects on multiphase burning in confined porous propellants. *Combust. Sci Technol.* **178**, 1685–1720.
- WAHLE, C. W. & MATKOWSKY, B. J. 2001 Rapid, upward buoyant filtration combustion waves driven by convection. *Combust. Flame* **124**, 14–34.
- WAHLE, C. W., MATKOWSKY, B. J. & ALDUSHIN, A. P. 2003 Effects of gas-solid nonequilibrium in filtration combustion. *Combust. Sci. Technol.* **175**, 1389–1499.
- WILLIAMS, F. A. 1985 *Combustion Theory: The Fundamental Theory of Chemically Reacting Flow Systems*. Perseus Books.
- WOOD, S. & HARRIS, A. 2008 Porous burners for lean-burn applications. *Prog. Energy Combust. Sci.* **34**, 667–684.
- ZHDANOK, S., KENNEDY, L. A. & KOESTER, G. 1995 Superadiabatic combustion of methane air mixtures under filtration in a packed bed. *Combust. Flame* **100**, 221–231.
- ZHU, D. L., EGOLFOPOULOS, F. N. & LAW, C. K. 1989 Experimental and numerical determination of laminar flame speeds of methane/(Ar, N₂, CO₂)-air mixtures as function of stoichiometry, pressure and flame temperature. In *Proceedings of 22nd Symposium (Int.) on Combustion*, pp. 1539–1545.